Astronomy with High Contrast Imaging III
M. Carbillet, A. Ferrari, and C. Aime (eds)
EAS Publication Series, 22 (2006) 261-280

DOI: 10.1051/eas:2006138

Very High Dynamic Range Imaging
Editors : will be set by the publisher
EAS Publications Series, Vol. ?, 2005

PUPIL REPLICATION

F. H. P. Spaan, E. Prot, V. Mourai and A. H. Greenaway[1]

Abstract. Pupil Replication is a technique which could be added to many existing high contrast imaging systems to improve the inner working angle or the contrast when using Pupil Replication. The output pupil of the telescope is replicated and mapped onto the input pupil of the high contrast imaging system. This decreases the size of the image of the star on axis and thereby increases the performance of the high contrast imaging system. In this paper the viability of such a system is assessed through mathematical analysis and simulations.

Contents

[1] School of Engineering and Physical Sciences, Heriot-Watt University, Edinburgh, United Kingdom

DOI: (will be inserted later)

1 Introduction

1.1 Context

The search for planets around nearby stars has become an active field of research since in 1995 the first indication of the existence such a system was found. Recently, at the European Space Agency 39^{th} ESLAB Symposium (2005) exo-planets were indicated as one of the major research areas for the coming decades.

Since the first discovery, about 150 so called exo-planets have been found, but all in an indirect way: by observed periodic radial or angular velocity changes of the star or apparent brightness changes; all believed to be due to an object orbiting the star in question. A first step beyond such indirect detections would be to observe light from the planet itself (reflected star light) that can tell, using spectroscopy, something about the composition of the planet. To achieve this, imaging of the planet is necessary, even if it is only as a point. Imaging such a planet is difficult because it is close to the star and, at visible frequencies, about 10^{10} times fainter than the star. Therefore imaging for exo-planet detection requires both high contrast imaging and a small inner working angle (IWA, the closest distance to the star a planet can still be observed). Several techniques have been proposed to achieve this, but they do not reach both the required contrast and IWA.

For most of these techniques Pupil Replication can be added between the telescope and the high contrast imaging system (HCIS) to reduce the IWA while maintaining the contrast performance. High contrast imaging systems to which PR could be applicable include apodisation techniques like aperture masks, image plane masks, coronagraphs and combinations as they are used in for instance the Terrestrial Planet Finder Coronagraph (see for instance Ford 2005) or the Lyot Project.

Using PR, the on-axis image of the star is decreased to a size smaller than the diffraction limit of the telescope, and off axis the point spread function (PSF) of the planet undergoes minor changes (not spectrally), contained within the envelope of the PSF of the telescope, see Greenaway et al. 2005. The principle of PR was proven experimentally and can be effected by a small-sized, low-complexity, high throughput optical system added between the telescope and the HCIS. We will now take a closer look at the principle of Pupil Replication.

1.2 Principle

The principle of pupil replication is illustrated in figure 1. The output pupil of the telescope is lead into the replication optics that replicates the pupil several times and then joins these replications. This new pupil is then lead into the input pupil

of the high contrast imaging system. On axis this works like an increase of the telescope diameter and decreases the size of the image of the on-axis star beyond the diffraction limit of the actual telescope.

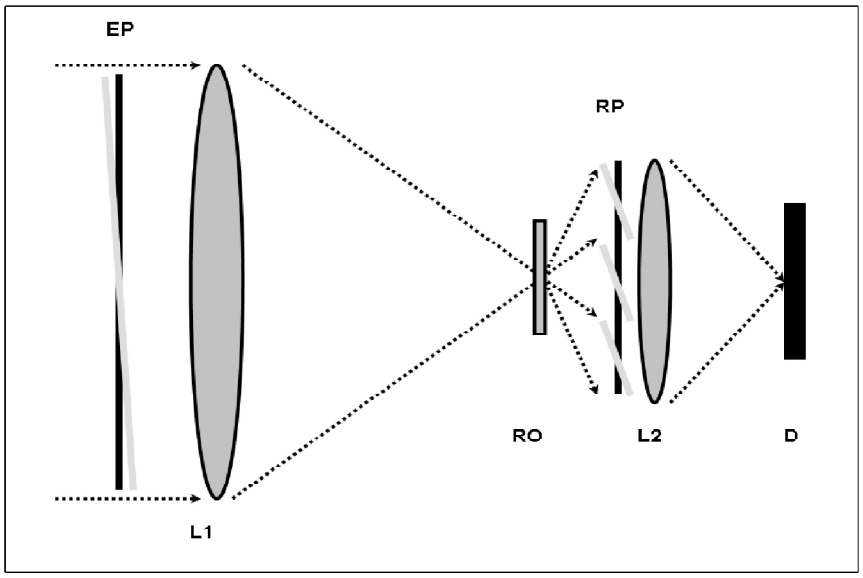

Fig. 1. A schematic overview of the principle of pupil replication. The wave front, after passing through the entrance pupil (EP), is focused by the optical system (L1) and then divided equally in amplitude 3 ways using the replication optics (RO). Thus 3 replicated images of the entrance pupil are formed side by side in the replication plane (RP), each 1/3 of the intensity of the original pupil image. If the source is an axial point the replicated wave fronts form a continuous plane wave front (solid black lines). If the source is off axis, the replicate wave fronts form a disjointed wave front (solid grey lines). The resulting wave front is then passed through an imaging system (L2) and an image of the point object is formed through this lens on the detector (D). The optical system L2 is presumed to incorporate the coronagraph or apodisation masks (not shown).

1.3 Imaging with Pupil Replication

We now look at the question: why is it that we can go beyond the diffraction limit? A key to the answer and the underlying principle of pupil replication is that one may violate the principles of homothetic mapping (a one-to-one relationship between input and exit pupil) whilst maintaining high-quality imaging performance over a small field of view. Beyond this field of view the imaging performance will be anisoplanatic, but when observing an exo-planet in this anisoplanatic region the reduced-quality off-axis image is an acceptable price to pay for improved dynamic range and a decreased IWA. Using pupil replication one may compress the image

of a star on axis whilst suffering only some chromatic (not spectral) defect in the uncompressed off-axis planet images. The compressed images of the on-axis star might, misleadingly, be thought of as 'super-resolved', but such 'super-resolution' is not information bearing, see for instance Toraldo di Francia 1955.

The effect of Pupil replication, and the way in which it complements other flux-suppression techniques such as coronagraphy or apodisation, is best explained by comparison with re-scaling the pupil. Whether or not the pupil is apodised, a simple re-scaling of the input pupil conserves the étendue, this is the product of area and divergence of the beam is constant. Thus re-scaling may change the size of the image (for instance to match it to detector pixels) but the ratio between the separation of image points and the width of the image PSF is preserved. By violating the homothetic mapping principle pupil replication alters this relationship, achieving a compression of the axial star image whilst preserving (subject to some chromatic defect) the angular position of an off axis source.

For an axial point source, if the replicated pupils are perfectly joined, the replicated wave front forms a continuous plane wave at all wavelengths (Figure 1, black lines), just like the re-scaled pupil. Thus, for an axial point source there is no difference between the images obtained by replicating the pupil or by re-scaling the pupil. If the source is re-imaged through the same lens, and the replicated input pupil diameter matches the re-scaled pupil diameter, both approaches yield an image with the same size, brightness and side-lobe structure. For an off-axis source the process of re-scaling the pupil leads to a change in the angle at which the radiation passes to the image plane through the re-imaging lens. Because the étendue is conserved, the angle at which the radiation passes through the lens varies inversely with the magnification of the pupil re-scaling. Thus, by demagnifying the input pupil one obtains a magnified image. If the source consists of two incoherent point sources the relative image width and the relative separation of the images is conserved.

In contrast, the replication procedure does not change the angle of divergence (beyond any change due to the demagnification of the pupil in a single replica). The exact location of the peak image intensity for an off-axis source now depends on the interference conditions established in the replicated pupils. For an off-axis source the violation of homothetic mapping means that there are discontinuities between the wave fronts in adjacent pupil replicas that arise from the same off-axis source point. The off-axis image is described by an envelope function equal to the image PSF through a single pupil replica and the detailed image structure within this envelope is determined by the interference conditions established by the discontinuous off-axis PSF. The precise number of diffraction peaks and their location within the envelope is determined by the properties of the replication and the wavelength. The envelope is always centred on the angle at which the off-axis point source would have produced an image in an un-replicated system when the re-scaled pupil has the same size as one of the pupil replicas. Thus, if the source consists of two incoherent point sources the relative image separation is preserved but the on-axis image is compressed and the off axis image chromatically smeared within an envelope whose width is determined by the resolution of the primary

pupil.

2 Analysis

2.1 Introduction

We analyse here the PSF of a pupil replication system. A one-dimensional case with three replications is assessed.

2.2 Three Replications in One Dimension

For an incoming on-axis plane wave, the image amplitude function produced by the Fourier Transform of the input pupil having a width d in one dimension is $sinc(x)$ $(= sin(x)/x)$. If we now replicate the pupil, each pair of replications added to the left and right of the unreplicated pupil adds a pair of δ functions in the pupil plane a distance $2d$ apart, see figure 2. So in the image plane the *sinc* function (which is the Fourier Transform of the original pupil wave) is therefore multiplied by a *cosine* function (the Fourier Transform of the pair of δ functions) plus a constant representing the original pupil. So the final expression for the amplitude is a *sinc* function multiplied by a sum of *cosine* functions, depending on the number of replications. For an even number of replications the same principle applies. So for 3 replications we have

$$T(x) = \frac{A}{\sqrt{3}}\Big(1 + 2cos(\frac{2d\pi x}{\lambda})\Big)sinc\Big(\frac{d\pi(x - sin(\alpha))}{\lambda}\Big) \tag{2.1}$$

where $T(x)$ is the image amplitude function, A is the amplitude of the incoming wave, d is the (unreplicated) pupil width and also the centre-to-centre pupil separation between pupil replicas, α is the view angle with respect to the optical axis, x is the coordinate in the image plane. The PSF is the modulus squared of the amplitude function T. These and following results are for non-overlapping replicas.

One can see from this equation that the *sinc* in the expression is displaced in x by a value dependent on the view angle α, but the *cosine* is unaffected by α: as the source moves off-axis, the *sinc* envelope moves relative to the *cosine* peaks, thereby modulating the *cosine* term. However, there is always a *cosine* peak on the optical axis. For all wavelengths, this one peak of the *cosine* pattern has the same position, but the positions of the other peaks change, depending on the wavelength. The actual peak amplitude of the off axis source is therefore position- and λ-dependent, but always confined within the displaced *sinc* envelope. It can be shown that for $\alpha > 3\lambda/d$ and broadband observations, there is practically no difference between the PSF of the planet with and without Pupil Replication.

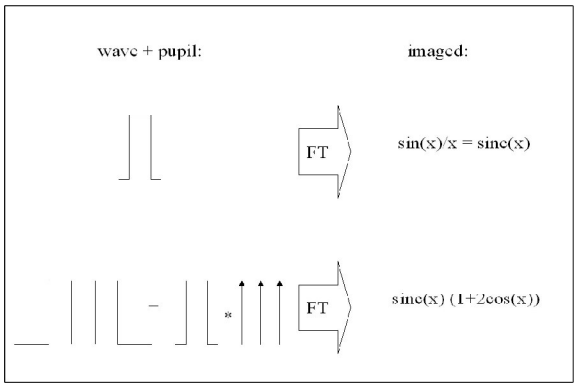

Fig. 2. The analytical scheme of Pupil Replication.

3 Pupil Replication and Hyper Telescope

In this section we look into the concept of the Hyper Telescope (see for instance Labeyrie 1996) with respect to the pupil replication system. We compare the two concepts and look at possibilities for combining them.

3.1 Comparison

Conceptually the Hyper Telescope is similar to Pupil Replication, see figure 3. Both deliver a number of pupil waves that are joined and then used as an input pupil for an imaging system. The main difference, which is shown in the figure, is that the Hyper Telescope has a piston term (phase offset) that is dependent on the baseline between the telescopes and on the view-angle α; the line connecting the pupils tilts in a direction opposite to the view direction. We will look into that in more detail.

An analytical comparison can be made when we take for the Hyper Telescope a one dimensional simplified situation where the telescopes are at equal distances apart, the distance between the optical centres of two telescopes being h. Similar results are obtained for more replications or telescopes and for larger values of h. We now need to change the $2cos()$ term in the sum over *cosines* in equation 2.1 and get instead

$$T(x) = \frac{A}{\sqrt{3}}\Big(1 + 2cos(\frac{2d\pi(x + (\frac{h}{d} - 1)sin(\alpha))}{\lambda})\Big)sinc\Big(\frac{d\pi(x - sin(\alpha))}{\lambda}\Big) \qquad (3.1)$$

The extra term $2d\pi((h/d) - 1)sin(\alpha)$ in the *cos* indicates that for the Hyper Telescope the peak of the cosine is not fixed to the optical axis, but suffers a wavelength independent shift to $x = ((h/d) - 1)sin(\alpha)$. For $h > d$ this shift is larger than the source displacement, as shown in figures 4 and 5 where for clarity instead of 3 replications or telescopes now 21 are used. One can see the central

peak behaves differently for a small ($< \lambda/d$) off-axis angle α. For large angles there is no particular difference to be seen. Furthermore the flux is smeared out but confined within the *sinc*-envelope of the single pupil (see figures 7 and 8). The behaviour for larger h is the same except that then the phenomena already occur at smaller angles (as can be seen from the equations where only h/d matters).

We also see from the analytical expressions for the Pupil Replication system and the Hyper Telescope system that on-axis ($\alpha = 0$) the PSF for Pupil Replication and the Hyper Telescope are the same (even though the spacing $h >> d$). The difference in PSF off axis means that the Hyper Telescope and Pupil Replication systems have fundamentally different application possibilities.

Another interesting phenomenon can be observed in figures 5 and 6. If we take the T of a Hyper Telescope, and a source at angle α, and now shift T in the x-direction by an amount $((h/d)-1)sin(\alpha)$, the *cosine*-term becomes zero and the *sinc* gets a total shift of $(h/d)sin(\alpha)$. This is the T of a Pupil Replication system viewing at an angle $(h/d)sin(\alpha)$. So in fact, the T of the Pupil Replication system at a view angle α_{PR} is equal to that of a Hyper Telescope viewing at an angle α_{HT} except for a shift; where for small angles $\alpha_{PR} = (h/d)\alpha_{HT}$ and the shift is $((h/d)-1)sin(\alpha_{HT})$. This is true for one point-source; for multiple sources the systems deliver different images. Furthermore, for coronagraphic systems suppressing on-axis sources, the mentioned shift also leads to different behaviour, even for one point-source.

In a Hyper Telescope system, which is normally used at $\alpha < \lambda/d$, so called chromatically smeared ghost images can appear. One can see this feature in figure 5 where the view angle is slightly off-axis to the right, the *cosine* peak is displaced to the left and from the right side a chromatically smeared ghost image appears. For Pupil Replication one sees in figure 4 that the *cosine* peak stays on axis. The ghost image appears only at an angle that is h/d times larger, see figure 6, with the central peak still on axis.

At angles higher than 1 λ/d Pupil Replication and the Hyper Telescope both start to behave similar to a single pupil telescope. Since this is the region where Pupil Replication is aimed to work, ghost images are not a problem for that system. The simulation results of Riaud et al. 2005 do not comply with this result.

3.2 Combination

The Hyper Telescope and Pupil Replication can also be combined. This is possible in the following two ways (see figure 9).

1) Each telescope of the Hyper Telescope can be equipped with a Pupil Replication system. We will call this system a Pupil Replicated Hyper Telescope (PRHT).

2) The combined pupil in the Hyper Telescope can be replicated there. This is a Hyper Telescope-like Pupil Replication System (HTPR).

In the case of a three-fold hyper telescope system and three-fold replication we can find the following equations:

$$T_{PR-HT} = \frac{T_{PR}}{\sqrt{3}}(1 + 2cos(\frac{2\pi(-3dx + (3d - h))sin(\alpha))}{\lambda})) \tag{3.2}$$

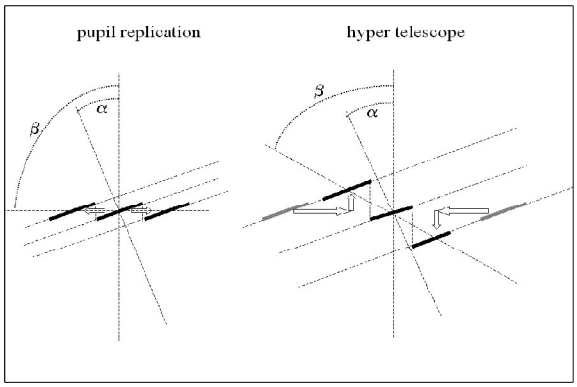

Fig. 3. The difference between the Pupil Replication (left) and the Hyper Telescope (right) principles, off axis, where α is the view angle.

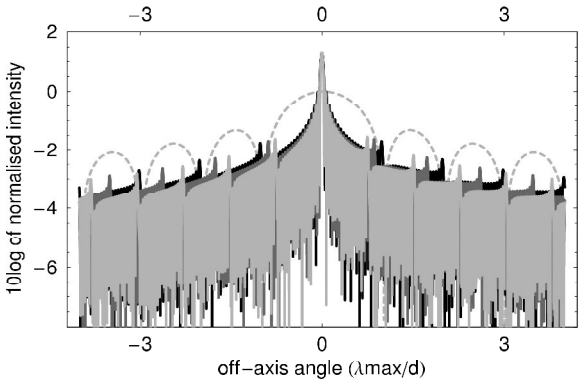

Fig. 4. The one dimensional analytical PSF of a 21-fold Pupil Replication system with an off-axis angle of $0.02\lambda/d$. Three wavelengths are shown: 1000, 872 and 760 nm in black, dark grey and light grey (the single pupil PSF dotted); $d = 2.5m$. One can see that the central peak stays on axis.

$$T_{HT-PR} = \frac{T_{HT}}{\sqrt{3}}(1 + 2cos(\frac{6d\pi(x - sin(\alpha))}{\lambda})) \tag{3.3}$$

where T_{HT} and T_{PR} are the amplitude function of the pupil replicated system and the Hyper Telescope respectively.

We see basically equations similar to those we have seen before. A result based on these equations is shown in the figure 10; note that in this figure the intensities for the three wavelengths have now been summed. In the case of PRHT (upper) the far off axis PSF is similar to that of both individual systems. However, we see that in the case of HTPR (lower), the cosine effect is taken into the PSF of the planet. Although this does not seem have an immediate use, looking into such

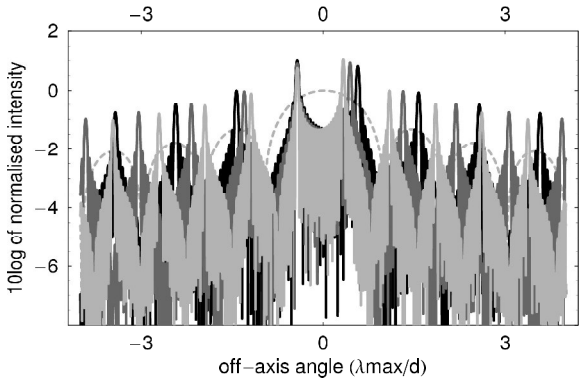

Fig. 5. The same situation as in figure 4 but now for the Hyper Telescope with $h = 22.2d$. One can see the central peak is displaced from the axis (in the opposite direction), and a chromatically smeared ghost image appear on the right side.

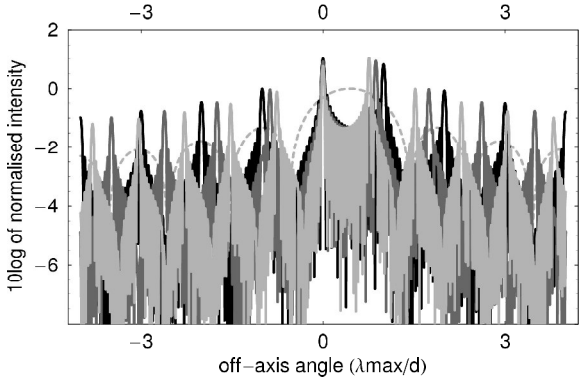

Fig. 6. The same situation as in figure 4 but now for an off axis angle of $0.444\lambda/d$. One can see a phenomenon similar to that of the Hyper Telescope but at an angle that is h/d times larger.

effects in more detail is subject of current research.

4 Simulation

Not all errors are amenable to analytic treatment and in this section we assess aspects of Pupil Replication by means of software simulations. We first describe the simulation procedure, then the results for a replicated pupil for rotation and magnification errors, for extended and finally for broadband sources.

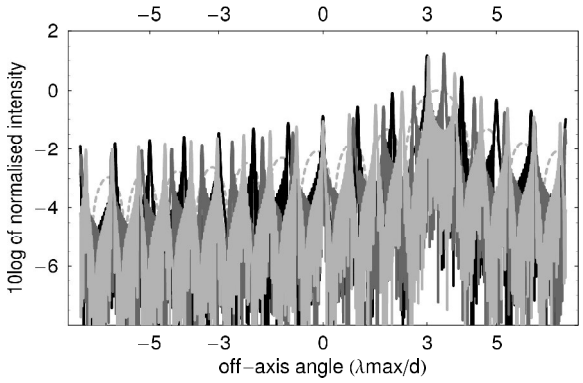

Fig. 7. The same situation as in figure 4 but now for an off-axis angle of 3.3 λ/d.

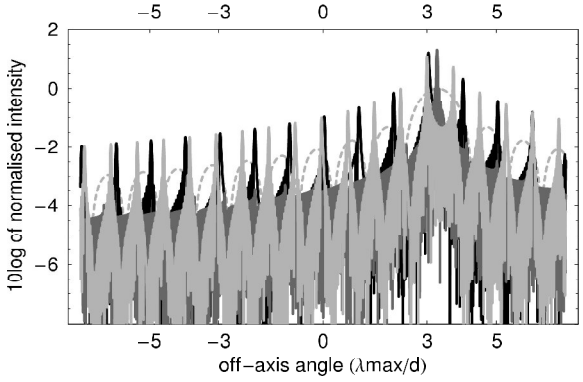

Fig. 8. The same situation as in figure 5 but now for an off-axis angle of 3.3 λ/d.

4.1 Procedure

The general procedure we used in these simulations consisted in the following steps:

1) Initialisation: for each wavelength, the pixel-scale (meters per pixel) has to be adapted because the Fourier Transform is essentially wavelength/pixel based. Furthermore, to effect the replication in the simulation we used a simulated perfect grating. Because the physical size of the pupil(s) and the grating used are fixed, the number of pixels to represent the pupil and the grating changes with the wavelength. Because of the finite pixel representation and -scaling, the overlap when summing different wavelengths is not perfect and gives rise to simulation results that are less good than the actual situation.

2) When required, an error can be applied at any of the following steps.

3) Create a vector representing a complex plane input wave arising from any

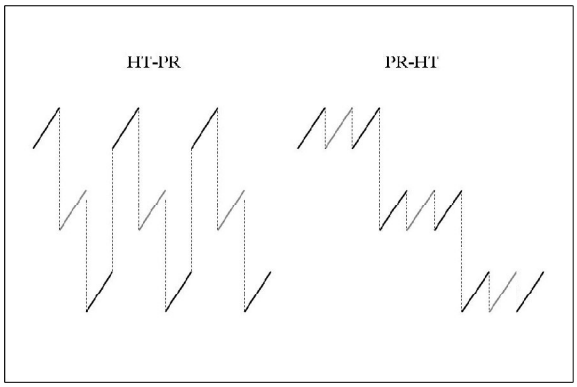

Fig. 9. Ways to combine the hyper telescope and pupil replication. On the left the hyper telescope scheme is implemented as indicated on the right in figure 3 and the hyper telescope arrangement is then replicated. On the right the array telescopes are individually replicated and these replicated telescopes are subsequently combined as a hyper telescope.

single angular direction in the object distribution at a specified wavelength.

4) Apply the first pupil, that is set the resulting complex distributions to zero outside a specified region that is substantially less than half of the vector, thereby representing an un-obscured and square telescope pupil of specified dimensions.

5) Perform a Fourier transformation on the resulting distribution, thus representing the image plane wave function at a specified wavelength.

6) Replicate the image plane wave function (pupil replication).

7) Apply a second pupil.

8) Fourier transform to produce the image wave function.

9) Apply the correction for the sampling (finite pixel-size) by multiplication of the Fourier Transform (*sinc*) of a single pixel.

10) Modulus square to evaluate the image intensity distribution from this single point source at this single wavelength.

11) Store this result.

12) Repeat the steps up to here for other sources, or for a grid of point sources making up an extended source (incoherent addition).

13) Repeat the steps up to here for a grid of wavelengths representing the desired wavelength band (incoherent addition).

14) Sum the intensity distributions over the source brightness distribution and over selected wavelengths.

When using more pixels in the calculations the minimum error in the optical system that can be simulated can be lower, because one pixel corresponds to a physically smaller unit. But because of reasons of computational and memory load, the obtained precision, especially in the error assessments later on, is limited by the maximum number of pixels that can be used to process this amount of

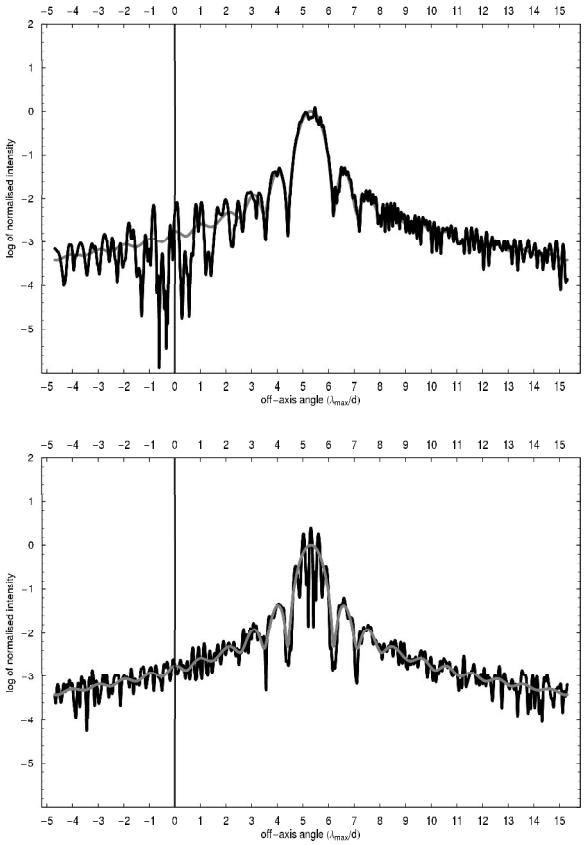

Fig. 10. PRHT (upper) and HTPR (lower) at an off-axis distance of 5.3 λ_{max}/d.

information in a practical amount of time.

4.2 Broadband Extended Sources

To find results for multiple wavelengths and extended sources, we have used simulations instead of mathematical treatment. Broadband results can be obtained by representing the wavelength band by a finite number of weighed monochrome PSFs and summing them. An extended source can similarly be represented by a grid of point-sources and their PSFs summed. Both can also be combined (nested) to get the image for a broadband extended source.

The image for an extended source using Pupil Replication is somewhat unusual and we therefore assess it in more detail here. We represented an extended source in our simulation by creating a grid of point sources, fine enough not to be resolved by the replicated optics. For reasons of computational load, a one-dimensional

simulation was used with 501 point sources, 0.01 λ/d apart, creating an extended source of 5 λ/d wide on axis. This simulation was done broadband, in the V-band, each source point represented by 8 weighted wavelengths. The non-replicated image shows a broad and flattened structure, as expected. The replicated source however shows regular peaks, not due to the representation grid of point sources but due to the replications; it is the same *cosine* that we saw in the analytical treatment of the PSF. From equation 2.1 we see that for 3 replications the *cosine* has peaks occurring every λ/d. As noted earlier, the positions of these peaks is not dependent on α and thus these peaks are manifest in the image of an extended source and are not smeared out as might have been expected.

For multiple wavelengths the chromatic effect tends to smear out the peaks, but since the central peak acts as the origin for the smearing it stays visible and broadens only. The side lobes are smeared out, but in the region close to the optical axis, the smearing effect does not lead to a flat profile. It is clear that this effect will become apparent for a source of $2\lambda/d$ or larger, that is when it would be resolved by the single pupil. For example, for a sun like star at $10pc$ observed at $500nm$ this effect would become noticeable with a telescope of $200m$ diameter.

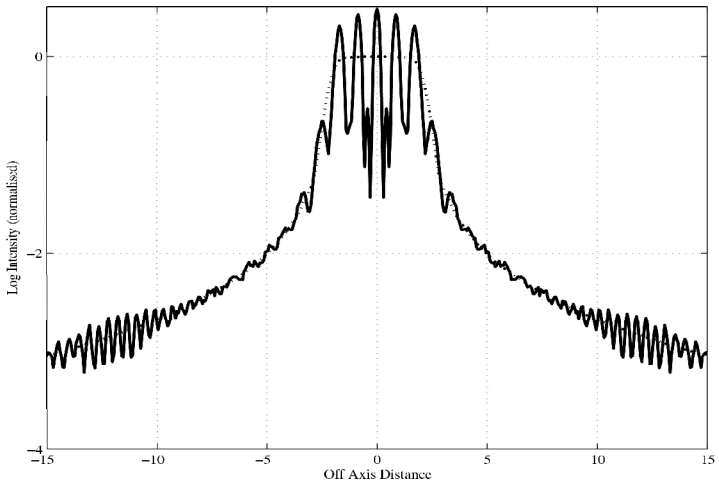

Fig. 11. An extended source of 5 λ/d simulated in one dimension with 501 point sources in the V-band with 8 weighed wavelengths. Shown are the image of the single pupil (dotted) and the image using a three-fold Pupil Replication (solid).

4.3 Replicated Pupil with Errors

We assessed errors in rotation and magnification of a pupil replica by simulating a system with two-fold pupil replication. One pupil (1) was on axis, the other pupil (2) joined to the right and on this pupil the errors were imposed. These simulations were done in one wavelength. The behaviour of more complicated

systems may be predicted from these results. The effect of other kinds of errors is subject of current research.

We simulated rotation errors in which pupil 2 is slightly rotated around the z-axis (z is the optical path direction) through its centre. Errors much smaller than at least one pixel shift at the edge are not meaningful when doing a simulation since the precision is limited by the pixel size. This value is $1/(pupilwidth/2)$, where *pupilwidth* is the width in pixels of the pupil in the simulation. One can however extrapolate the results shown in figure 12 to lower values. These results demonstrate that the losses are not too serious unless significant rotations are experienced.

We also simulated magnification errors at different levels, where pupil 2 is slightly (de-)magnified (the centre of magnification being the centre of the pupil). The results are shown in figure 13 and show that the loss in sensitivity due to magnification errors can be serious. This indicates a need to ensure, as far as possible, that no non-common path elements having optical power should be included in the experimental arrangement.

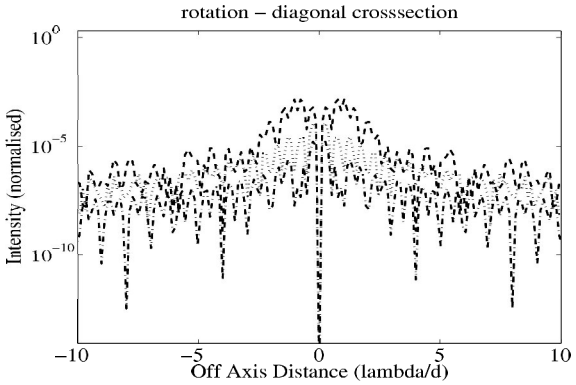

Fig. 12. Cross-section (diagonal) through the two-dimensional simulated difference image at different levels of the rotation error: .1/33, 1/33 and 10/33 radians (shown as dash-dotted, dotted and dashed respectively).

4.4 Coronagraph

In Greenaway et al. 2005 we showed results for a pupil apodised coronagraph simulated in one dimension and one wavelength. We show here further results: we assess the effect of a star stop, and of broadband observations. We also look at the effect of random optical errors and the dependency of these results in particular on the pixel size of the simulation. We simulated specifically the following:

1) an on-axis star and an off-axis planet observed with a telescope with 3-fold pupil replication and super Gaussian pupil apodisation,

2) the same situation including a star stop

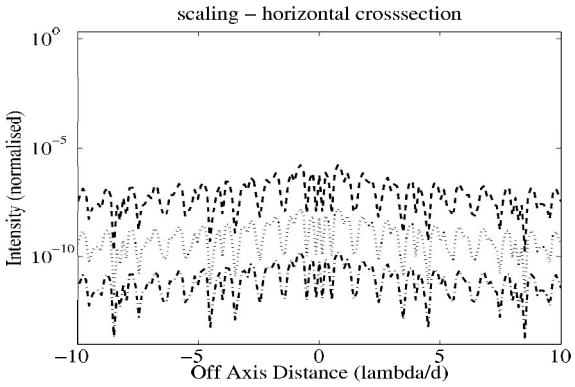

Fig. 13. Cross-section (horizontal) through the two-dimensional simulated difference image at different levels of the magnification error: a magnification of $(1-1*10^{-9})$, $(1-1*10^{-7})$ and $1-(1*10^{-5})$ (shown as dash-dotted, dotted and dashed respectively).

3) also star stop and in broadband,

4) including random amplitude and phase errors on the single pupil

5) and the dependency of these results on the pixel size.

In figure 14, left, is shown the result in one wavelength for an on-axis star and a planet at about 7 λ/d (10^{10} times fainter) for a normal telescope (dotted line), an apodised system (super Gaussian, dashed line) and for a 3-fold pupil replicated apodised system (solid). Only in the PSF of the pupil replicated apodised system the planet appears. If a star stop is added to this system, two times $4\lambda/d$ wide, we get the result shown in figure 14 (right). Because of the scattering of the star light at the star stop edge the planet is now barely visible.

In figure 15 (left) the result is shown for a bandwidth of $\delta\lambda/\lambda = 0.25$, represented by 8 wavelengths. The axis scale is in λ/d of the largest wavelength. The scattered star light has now relatively decreased, because for shorter wavelengths, the star stop appears to be larger and stops more light.

When errors are introduced, the side lobes will rise. This is shown in figure 15 (right), where a relative random amplitude error is introduced to the pupil wave of 3×10^{-5} together with a random phase error of 3×10^{-6} waves. This brings the side lobes up to a value of 10^{-12}.

Although it appears confusing in this one-dimensional representation, the artefact due to the star will have a circular symmetry and can thus be distinguished from the planet image.

Because we have to work with a finite pixel size, there is a limit on the smallest error length (over the pupil) we can introduce. The effect of this is shown in figure 16 where respectively 4 times less and 4 times more pixels have been used to represent the image and the pupil. It follows from this that the values of 3×10^{-5} and 3×10^{-6} for the errors to stay below 10^{-12} are upper limits: a larger simulation (more pixels) will relax the error constraint values and be closer to reality.

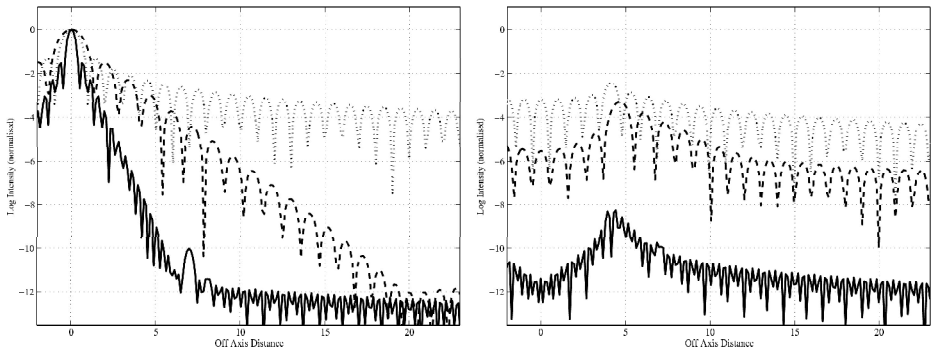

Fig. 14. Left, a simulation result in one wavelength and one dimension for a star on axis and a planet at about 7 λ/d (10^{10} times fainter) for a normal telescope (dotted line), an apodised system (super Gaussian, dashed line) and for a 3-fold pupil replicated apodised system (solid). On the right side the same but now including a star stop of $2x4\lambda/d$.

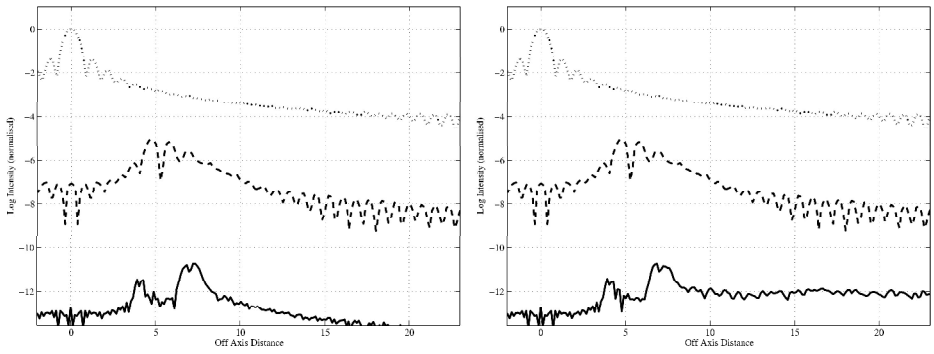

Fig. 15. On the left: like figure 14, but in broadband (see text). On the right the same but now with an error imposed on the input pupil (see text).

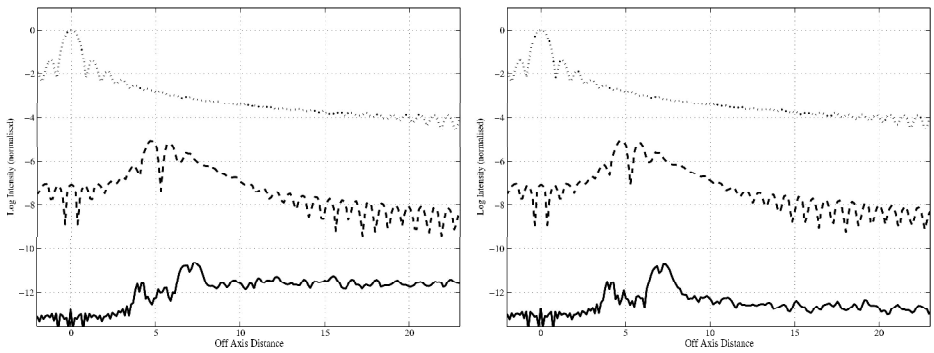

Fig. 16. Like figure 15, but now using a smaller (left) or larger (right) number of pixels.

4.5 Statistical Errors

The effects of the turbulent atmosphere on the efficiency of the suppression of the starlight in Pupil Replication can be estimated. For a single pupil telescope the uncompensated (by adaptive optics) turbulent wave front variance is of the order of $(D/r_0)^{5/3}$, see for instance Tyson 1998. If we look at a three-fold Pupil Replicated system, the same wave-front appears three times and joined to each other. This means that the variance does not change significantly when introducing Pupil Replication in the case of a turbulent atmosphere.

5 Experimental and Optical Design Issues

One of the parts of Pupil Replication that have not been assessed so far is the design for the optics that produce the replications of the pupil. A possible design for 2-fold replication of a rectangular input pupil is given here, see figure 17. The light entering from the top is split using a beam splitter. The two beams are then guided further using mirrors to be recombined. The last two mirrors are fixed to a translating element to change the beam separation. If we estimate the general efficiency of a mirror as 97%, the overall efficiency is about 88%. Such optics can be put into solid glass (except for the last two mirrors). Furthermore, using the last two mirrors as shown, it is possible to eliminate a gap or overlap error. Finally, this system can be cascaded to obtain 2^n replicas.

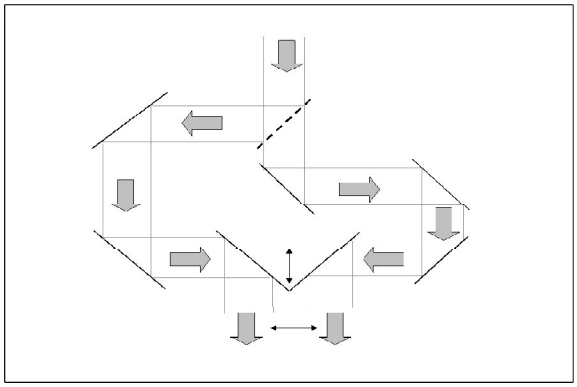

Fig. 17. A design for the replication optics.

An experiment was set up to test our theoretical model of pupil replication, see figure 18. Although pupil replication is meant to replicate the pupil in a telescope, we used for simplicity a laser beam instead of a telescope pupil to create the incoming wave front. The basic set up is that of a Mach-Zehnder interferometer, but instead of combining the two interferometer beams at the exit pupil so that they overlap, the beams were sheared with respect to each other. This way two disk shaped monochrome wave fronts are created at the exit pupil. These represent

the replicated pupils in a telescope with pupil replication. In the experiment the two beams are then both imaged onto a detector through a single lens, as would be the case when applied to a telescope.

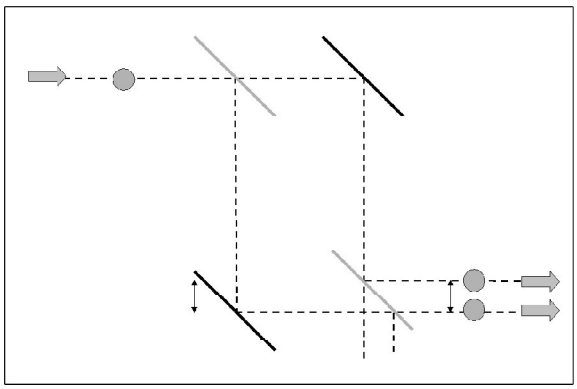

Fig. 18. The experimental set up.

Figure 19 shows a typical set of images that were obtained. The top left picture shows part of the beam at the exit pupil, the poor quality of the beam is visible; the optics used were of moderate quality. The interference in the right part of this picture is due to the other pupil replica. On the top right the cross section through this pupil image is shown. The second and third rows show the unreplicated PSF of each of the beams. The fourth row shows the decreased size of the PSF in the replicated system (shown later in more detail). The last image is saturated to show the side lobes of the replicated PSF.

We also simulated the experimental set up and then compared the simulation results with the experimental results. We show here two cases at different values for the separation between the two pupil replicas (shear of the beams in the interferometer). In the figures only the cross sections through the two dimensional PSFs are shown.

In the left figure of figure 20 the separation is zero, that is the two discs are just touching each other. For the central and first order peaks the agreement between simulation and experiment is good; the third peaks come close to the lowest level of the CCD detector and the match here is less good; they are also subject to greater error.

On the right in figure 20 the separation is half the width of the beam, that is the two discs half overlap. Again, for the central and first order peaks the agreement between simulation and experiment is good, and for the third peaks less good. We also see that the central peak is now broader and the side lobes lower; this is because the separation is less than in the previous case.

Finally some remarks about the experiment. The beam shape had a soft edge so that the experimental determination of the beam separation was difficult. In practise we adjusted the separation in the simulation to give a best fit of the PSFs.

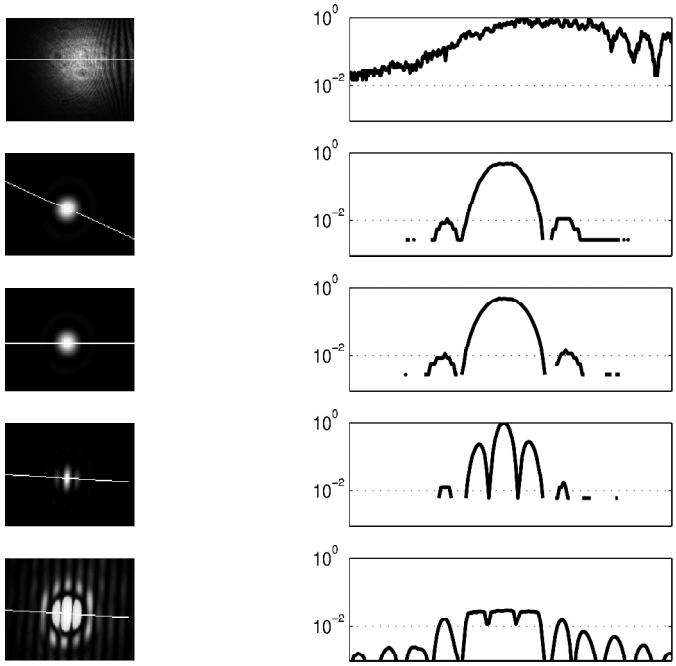

Fig. 19. Experimental pictures (see text).

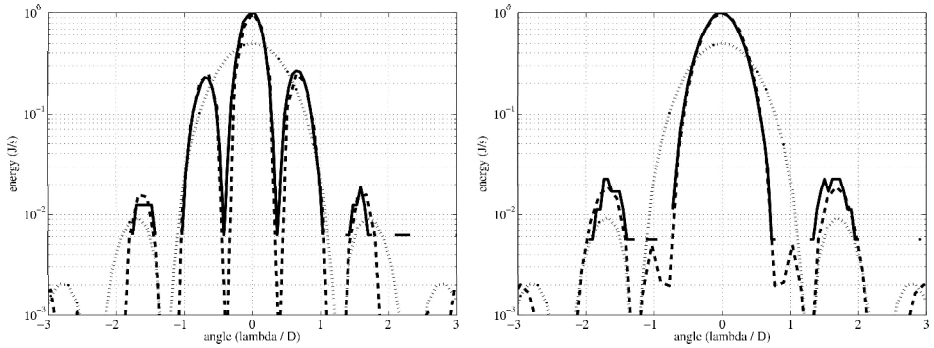

Fig. 20. Left: Pupil replicas in contact (see figure 19): comparison with simulation results. Cross sections are shown of the simulated unreplicated PSF (dotted), of the simulated replicated PSF (dashed) and of the experimental replicated PSF (solid). Right: the same but now with half overlapping pupil replicas.

In our simulation we used a beam with a hard edge; a soft edged beam did not give better results. The saturated images we obtained gave more information on the higher order peaks, but a good fit with the simulation could not be obtained.

The quality of the optics and other equipment used limited the results in this way. To get a better fit than shown, the optical defects would have to be taken into account in the simulation. Although imperfect, these experimental results give us confidence in our simulation.

6 Discussion

In the efforts to try and reach the 10^{10} dynamic range region, pupil replication can relax the requirements posed on the instrument to be built. In this paper we have assessed several aspects of pupil replication; the results point in the direction of feasibility. They encourage us to look further into such a system and work towards analysis and simulation of pupil replication applied to specific system designs as they are emerging from the projects that aim to try and image extra solar system planets.

References

39th ESLAB Symposium 'Trends in Space Science and Cosmic Vision 2020, 19-21 April 2005, European Space Agency, Noordwijk, the Netherlands

Greenaway, A. H., Spaan, F. H. P. & Mourai, V. 2005, ApJL, 618-2, L165

Labeyrie, A. 1996, A&AS, 118, 517-524

Riaud, P., Mawet, D. & Absil, O. 2005, ApJL, 628-2, L81

Toraldo di Francia, G. 1955, Journal of the Optical Society of America, 45, 497-501

Ford, V. 2005, editor, *TPF Coronagraph Flight Baseline 1 Design Interim Status Report*, Jet Propulsion Laboratory

Tyson, Robert K. 1998, *Princples of Adaptive Optics*, second edition, Academic Press